ASSESSMENT OF BIOCHEMICAL, HISTOLOGICAL CHANGES AND TISSUE EXPRESSION OF P53 AS INDICATOR OF EARLY POSTMORTEM INTERVAL IN ADULT MALE ALBINO RATS

Sara E. Kasem [1], Soheir A. Mohamed [1], Samira M. Mohamed [2], Martena Osam Khalaf [1], Ahmed M. Said [1]

[1] Department of Forensic Medicine and Clinical Toxicology, [2] Department of Histology and Cell Biology, Faculty of Medicine, Sohag University, Egypt

Corresponding Author:
Sara E. Kasem. **Mobile:** 01092635906. **E-mail:** Saraalsayed@med.sohag.edu.eg.

Submit Date 2023-05-16
Revise Date 2023-08-13
Accept Date 2023-08-15

ABSTRACT

Background: Estimating the period since death is forensic medicine's primary priority. It assists other judicial inquiries in comprehending the situation and accounting for prospective offenders. **Objectives:** The current research is attempting to evaluate the role of various methods in the estimation of the postmortem interval by studying the biochemical changes in the blood (serum levels of uric acid, lactate, amylase, lipase, and insulin), histological changes, and anti-p53 antibody immunohistochemical expression in the tongue and pancreas. **Methodology:** Forty adult male Albino rats served as the subjects for the current investigation. According to varied postmortem intervals, the animals were randomly divided into four groups: 0 hours, 12 hours, 24 hours, and 48 hours after death. **Results:** The postmortem interval, serum uric acid, lactate, and lipase displayed a significant positive correlation. Time-dependent alterations could be observed in the pancreatic and tongue histological sections. Anti-p53 antibody immunohistochemistry expression increased progressively over the postmortem period. **Conclusions**: Determining how long has transpired after death is essential in forensic medicine. The serum lactate level is the most accurate of the studied biochemical parameters. Additionally, regression formulas using the optical density scores of the tongue and pancreas can be used to forecast PMI more accurately when combined.

Keywords: Postmortem interval, Postmortem biochemistry, Apoptosis, p53

INTRODUCTION

As a cell dies, the physiological processes that keep it intact and functioning stop. The body starts a continuous, irreparable sequence of chemical and physical alterations after death **(Brooks and Sutton, 2018).** In the early postmortem (PM) hours, physical changes can be seen, such as the start and lapse of rigor mortis, the advancement of livor mortis, and algor mortis. The main composition of several body fluids also changes in other ways **(Cordeiro et al., 2019).**

Several considerations should be kept in mind while estimating the period since death. Many elements, such as ambient temperature, humidity, soil temperature, and soil salinity, impact the physical and chemical changes after death **(Onyejike et al., 2022).**

The postmortem interval (PMI) is the period between the time of death and the time the body is found (**Abdelaleem et al., 2016).**

Determining how long has elapsed since death is the primary objective in forensic medicine. It aids in understanding the circumstances and identifying potential criminal suspects **(Welson et al., 2021)**. It is occasionally hard to pinpoint the precise moment of death based on the development of a single postmortem change **(Mohamed et al., 2020).**

Most recent forensic research has focused on the biochemical alterations in bodily fluids, including vitreous humor, cerebrospinal fluid (CSF), and synovial fluid, after death **(Yahia and Abdel-Hakiem, 2014).**

For reliable PMI estimations, histological and immunohistochemical examination of detrimental alterations in body organs has emerged and been integrated with other techniques **(Welson et al., 2021).**

A carefully controlled form of cell death called Apoptosis encourages the clearance of dying cells from healthy tissues. This type of cell death is a crucial biologic mechanism contributing to healthy tissue homeostasis and appropriate development. **(Elvas et al., 2019).**

When a cell is injured, the ubiquitous tumor suppressor protein p53 is usually activated. It participates in several signaling pathways that control cell survival and death

(Tang and Zhang, 2017).

The objective of the current study is to assess the contribution of various methods in postmortem interval (PMI) estimation by examining blood biochemical changes (uric acid, lactic acid, amylase, lipase, and insulin), histological changes, and immune response to the apoptotic marker anti-p53 antibody in the tongue and pancreas.

The extent of histological abnormalities in the tongue and pancreas has been correlated with PMI in previous studies. However, there have been very few immunohistochemistry investigations conducted so far.

The current study could be the first to evaluate tongue immunohistochemistry alterations to estimate the elapsed period since death.

MATERIAL & METHODS

Type of study: Experimental animal study.

Experimental rats: Forty mature male Albino rats used in this investigation ranged in weight from 100 to 200 g. They were provided by the animal facilities center of the Faculty of Agriculture at Cairo University, Egypt. Animals were housed in metal cages at the Faculty of Medicine, Sohag University. The animals spent a week getting used to the lab environment before being tested. They were given water and typical pellet food. The investigation was carried out in December 2021.

Ethical consideration: The ethical and animal husbandry standards related to animal research were considered according to the guidelines for handling and using laboratory animals established by the Medical Research Ethics Committee of the Faculty of Medicine, Sohag University. IRB registration number: Soh-Med-21-12-03.

Study design: The animals were divided at random into 4 groups, each consisting of ten rats: Group I (0-hour PM), Group II (12 hours PM), Group III (24 hours PM), and Group IV (48 hours PM), according to various postmortem intervals. At the start of the study, all animals had been anesthetized before being sacrificed. The dead animals were incubated at room temperature (22 ± 2 °C) and 50% humidity.

Evaluation of biochemical changes in blood: The blood was drawn from the anesthetized rats via cardiac puncture on the left side and placed into a 5-ml ethylene diamine tetraacetic acid (EDTA) collection tube using a 5-ml syringe. All blood samples were stored in vitro at room temperature (22 ± 2 °C) and 50% humidity for postmortem intervals **(Donaldson and Lamont, 2013)**. At different postmortem intervals, the blood samples were centrifuged using a centrifuge apparatus, Hettich Zentiugen model EBA20, for separation of the serum for later evaluation of the level of uric acid, lactate, amylase, lipase, and insulin using Clinichem1 (a spectrophotometer) and ELAN 30's fully automated microstrip ELISA processor.

Evaluation of histological changes

The tongue and pancreas were removed at various postmortem times and immersed in a 10% formalin solution. The samples underwent processing before being paraffin wax embedded. Five sections—each 30 μm thick—were taken from each organ using a microtome. Hematoxylin and eosin were used to stain the samples. Then, an Olympus CX-41 RF microscope was used for microscopic inspection.

Immunohistochemistry staining protocol: The avidin-biotin-peroxidase complex (ABC) technique was utilized to perform immunohistochemistry (IHC) on paraffin slices of tongue and pancreatic tissues placed on positively charged slides. A polyclonal rabbit anti-p53 antibody (Elabscience Cat# E-AB-67701, Dil.1:50) was applied in this IHC investigation. Sections from each group were treated with the corresponding antibody before the essential reagents for the ABC technique (Vectastain ABC-HRP kit, Vector laboratories) were added.

Marker expression was colored with diaminobenzidine (DAB, manufactured by Sigma) and peroxidase-labeled for recognizing antigen-antibody complexes. For the negative controls, non-immune serum was used instead of the primary or secondary antibodies. A Leica microscope (CH9435 Hee56rbrugg; Leica Microsystems, Switzerland) was used to view IHC-stained sections.

Immuno-scoring by optical density measurement: Quantitative evaluation was done by screening the pancreatic and tongue samples and choosing at least six areas for each group under investigation. By calibrating the Leica Qwin 500's image analysis system (LEICA Imaging Systems Ltd. Cambridge, England), the optical density of p53 positive cells was ascertained.

Statistical analysis: The Kolmogorov-

Smirnov test of normality was used to determine if the data were normal. This test's results indicated that most data were parametric and normally distributed; thus, descriptive analysis, one-way ANOVA, and post-hoc testing were conducted to determine the intergroup relation. The Pearson correlation coefficient test and linear regression analysis were used to assess correlations. When the p-value is less than 0.05, significance is considered. SPSS 21.0 (Statistical Program for Scientific Studies, SPSS, Inc., Chicago, IL, USA) for Windows was used for the statistical analysis.

RESULTS

Biochemical results

The mean serum uric acid and lactate levels in groups II, III, and IV were statistically significantly higher than in group I (p-value < 0.001). The mean serum amylase values in groups II, III, and IV showed a non-significant. gradual increase (p-value 0.55).

The rise of serum lipase occurred at 24 hours, with no further increase at 48 hours. The mean serum lipase levels in groups III and IV showed a statistically significant rise compared to group I (p-value 0.001). The research groups' average serum insulin levels showed no apparent change, p-value 0.77 (Table 1).

The strongest positive correlations were observed between serum lactate, lipase, uric acid, and PMI (r = 0.86, 0.71, and 0.70, respectively, p-value < 0.001). However, there was a non-significant correlation between serum amylase, insulin, and PMI, p-value 0.15, 0.61 respectively **(**Table 2).

A regression formula was obtained to predict PMI from serum lactate. PMI= 0.052 + 0.111 (serum lactate). It has a high predictive value, with an adjusted R^2 of 74% (Table 3).

Table (1) Comparison of postmortem serum uric acid, lactate, amylase, lipase, and insulin

Groups	Uric acid (µmol\L)	Lactate (mmol\dl)	Amylase (U\L)	Lipase (U\L)	Insulin (mu\ml)
			Mean ± SD*		
Group I (0 h)	154.88 ± 54.05[b c d]	8.89 ± 2.72[b c d]	567.73 ± 142.67	29.22 ±10.16 [cd]	0.16 ± 0.03
Group II (12h)	284.43 ± 41.46[a]	23.11 ± 2.39[a d]	623..68 ± 197.66	56.68 ± 18.13	0.16 ± 0.01
Group III (24h)	290.12 ± 41.23[a]	26.19 ± 5.28 [a]	695.16 ± 291.10	85.12 ± 28.03 [a]	0.17 ± 0.02
Group IV (48 h)	300.67 ± 43.97[a]	30.07 ± 4.38 [a b]	700.6 ± 129.33	86.95 ± 34.96 [a]	0.16 ± 0.02
P-value	< 0.001*	< 0.001*	0.55	0.001*	0.77

*SD: standard deviation. **significant p-value < 0.05 .[a] significant when compared to group I. [b] significant when compared to group II. [c] significant when compared to group III. [d] significant when compared to Group IV

Table (2) Pearson's correlation coefficient for the correlation between PMI and serum levels of uric acid, lactate, amylase, lipase, and insulin

	Correlation coefficient factor (r)	P value
Uric acid	0.70	< 0.001**
Lactate	0.86	< 0.001**
Amylase	0.300	0.15
Lipase	0.71	< 0.001**
Insulin	0.109	0.61

**Correlation is significant at the 0.01 level.

Table (3): Multivariate linear regression (backward) to predict PMI.

	Model	Unstandardized Coefficients		Standardized Coefficients	T	Sig.	Adjusted R^2
		B	Std. Error	Beta			
1	Constant	-0.142	0.467		-0.304	0.764	75%
	Uric	0.002	0.003	0.097	0.569	0.576	
	Lactate	0.090	0.027	0.696	3.378	0.003*	
	Lipase	0.004	0.006	0.121	0.705	0.489	
2	(Constant)	0.052	0.333		0.157	0.877	74%
	Lactate	0.111	0.014	0.860	7.890	<0.001*	

*significant p-value < 0.05. PMI = 0.052 + 0.111 (serum lactate).

Tongue histological and immunohistochemical results

Histological examination of H&E-stained tongue sections excised immediately after death showed that the ventral aspect of the tongue was covered with keratinized stratified squamous epithelium, and the lamina propria in the tongue was formed of dense connective tissue (CT) that was rich in blood vessels. In the middle of the tongue, the muscle appeared in different directions, which represent the supporting tissue of the tongue (Fig.1A). At 12 hours PM, there were cytoplasmic vacuolation, karyolysis, and pyknosis in the superficial and spinous layers of the epithelium of the ventral aspect of the tongue with CT homogenization (Fig. 1B).

At 24 hours after death, the ventral aspect of the tongue revealed epithelial shredding and splitting. The epithelium showed pyknosis and karyolysis throughout the epithelium. There was also muscle degeneration (Fig. 1C). At 48 hours, a microscopic examination of the tongue section revealed the ventral aspect of the tongue with epithelial shredding, splitting, and pyknosis throughout the epithelial thickness. There was also extensive muscle degeneration (Fig. 1D).

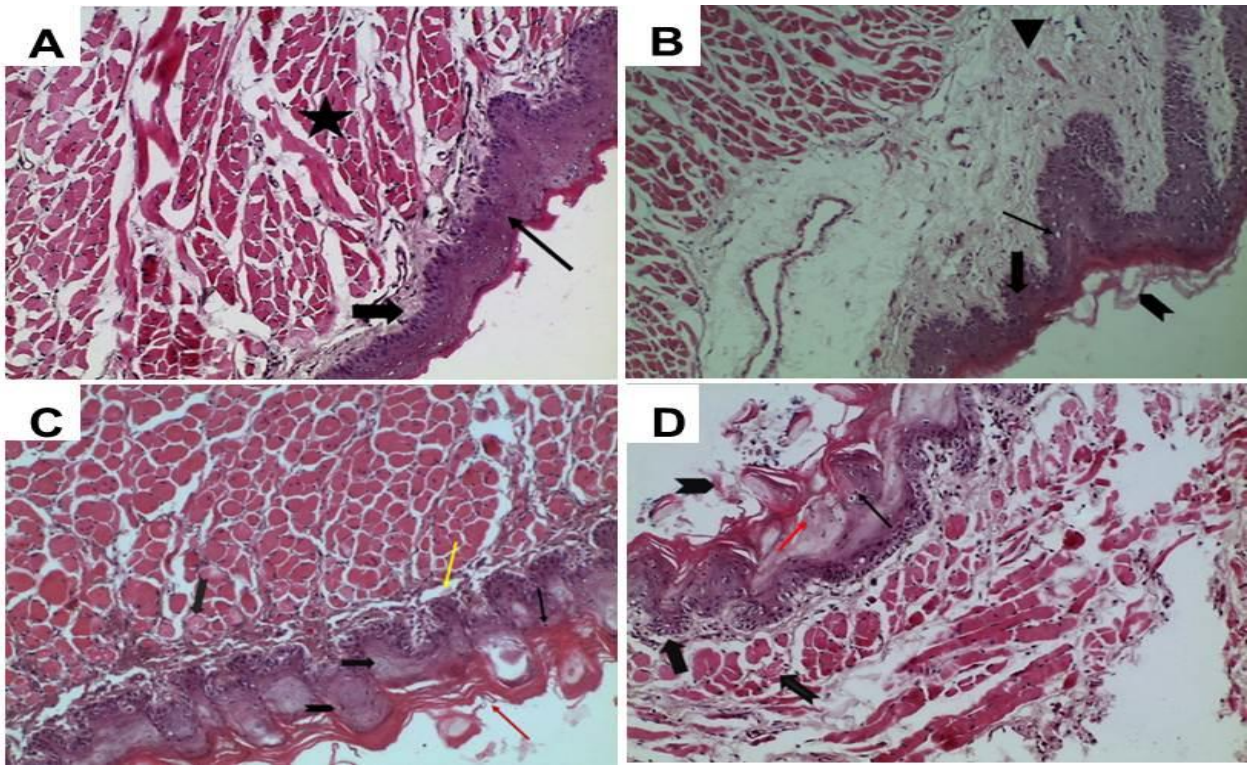

Figure (1): Histological changes of the tongue at different postmortem intervals

(A): A photomicrograph of a tongue section of an adult male rat from group I show the ventral aspect of the tongue with the epithelium (thin arrow), lamina propria (thick arrow), and muscular core (star). (H, E stain x 200).

(B): A photomicrograph of a tongue section of an adult male rat from group II showing the ventral aspect of the tongue with epithelial shredding (chevron arrow), karyolysis (thin arrow), and pyknosis (thick arrow) in the superficial and spinous layers with CT homogenization (arrowhead). (H&E stain x 200).

(C): A photomicrograph of a tongue section of an adult male rat from group III showing the ventral aspect of the tongue with epithelial shredding (red arrow) and splitting (yellow arrow). The epithelium showed pyknosis (thin arrow), karyolysis (chevron arrow), and karyorrhexis (thick arrow) throughout the epithelium. There was muscle degeneration (intended arrow). (H, E stain x 200).

(D): A photomicrograph of a tongue section of an adult male rat from group IV showing the ventral aspect of the tongue with epithelial shredding and splitting (thick arrow). The epithelium showed pyknosis (thin arrow) and karyorrhexis (red arrow) throughout epithelial thickness. There was muscle degeneration (intended arrow). (H, E stain x200).

Immunohistochemically stained sections of the tongue in group I exhibited scarce cytoplasmic reactivity along skeletal muscle cells to the p53 antibody (Fig. 2A). A section of the tongue in group II revealed moderate expression of the p53 antibody as a cytoplasmic reaction on skeletal muscle cells (Fig. 2B). A section of the tongue in group III displayed high cytoplasmic reactivity of the p53 antibody to most skeletal muscle cells (Fig. 2C). A section of the tongue in group IV is highlighted by the extremely intense cytoplasmic reactivity of the p53 antibody on some lining epithelial cells as well as skeletal muscle cells (Fig. 2D).

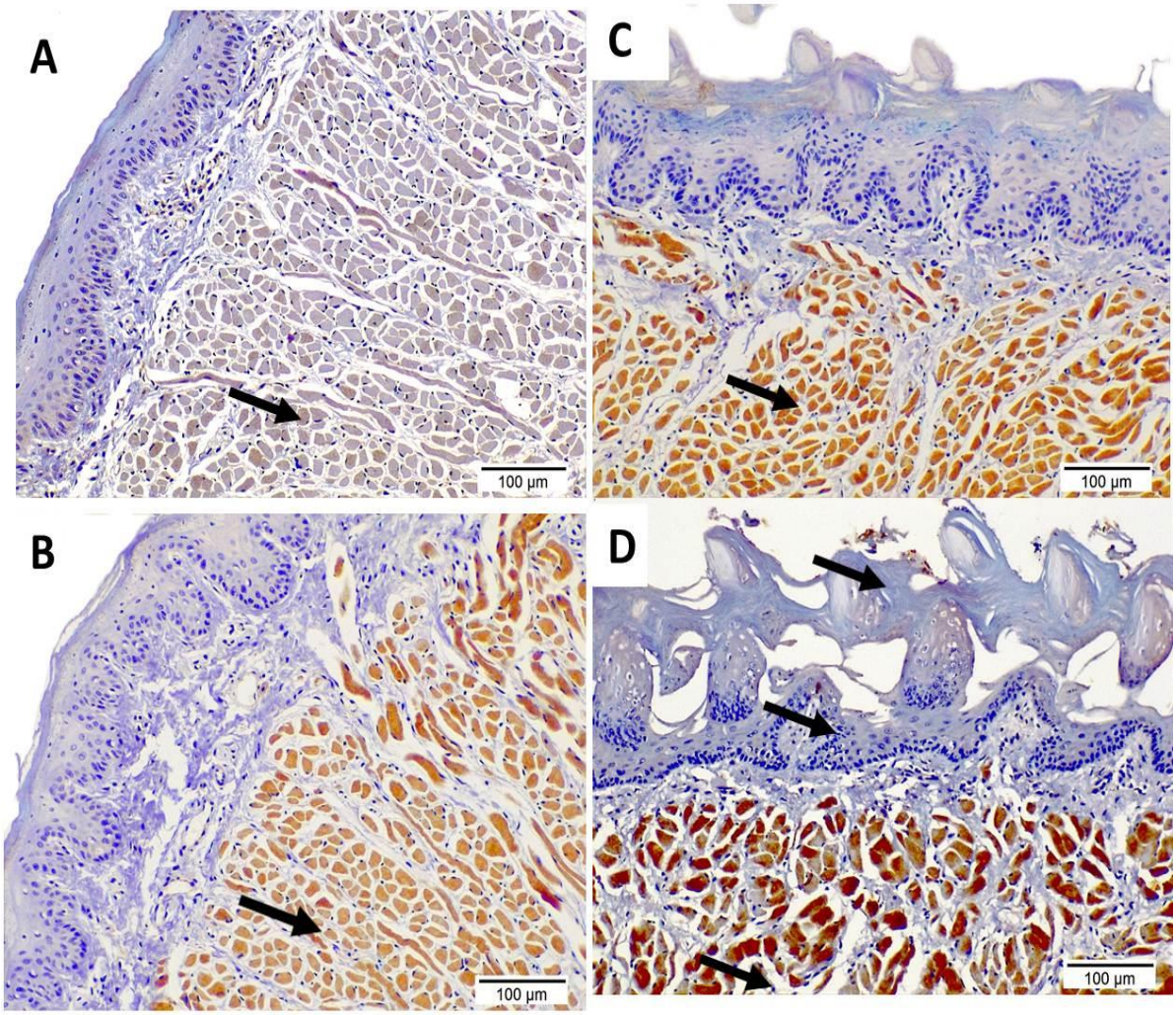

Figure (2): Photomicrographs present the expression of P53 antibodies on the tongue tissues among the studied groups.

(A): A section of the tongue in group I exhibited scarce cytoplasmic reactivity along skeletal muscle cells to the p53 antibody (arrow).

(B): A section of the tongue in group II revealed moderate expression of the p53 antibody as a cytoplasmic reaction on skeletal muscle cells (arrow).

(C): A section of the tongue in group III displayed high cytoplasmic reactivity of the p53 antibody to most skeletal muscle cells (arrow).

(D): A section of the tongue in group IV is highlighted with the extremely intense cytoplasmic reactivity of the p53 antibody on some lining epithelial cells and skeletal muscle cells (arrows). (P53 antibody, magnification power = x200, and scale bar = 100 m).

With rising PMI, the optical density score values of the tongue's p53-positive cells statistically significantly increased (Table 4, Graph 1). The tongue p53 optical density score and PMI exhibited a strong positive correlation (r 0.98, $p < 0.001$) (Table 5). Simple linear regression was applied to develop the following equation to predict PMI: PMI = 0.406 + 5.820 * P53 optical density score of the tongue, with an adjusted R^2 of 96.9%. (Table 6).

Table (4): The optical density scoring differences of P53 between studied groups.

Tissue	Mean ± SD				F value	P- Value
	Group I (n = 10)	Group II (n = 10)	Group III (n = 10)	Group IV (n = 10)		
Tongue	0.096 ± 0.011 ^ # +	0.303 ± 0.047 * ^ #	0.43 ± 0.04 * + #	0.61 ± 0.029 * ^ +	116.677	< 0.001
Pancreas	0.049 ± 0.023 ^ # +	0.277 ± 0.047 * ^ #	0.507 ± 0.047 * + #	0.729 ± 0.035 * ^ +	166.637	< 0.001

Values are expressed as mean ± SD. * refers to a significant difference from group I; + refers to a significant difference from group II; ^ refers to a significant difference from group III; and # refers to a significant difference from group IV. A significant difference was presented at $p < 0.001$.

Table (5): Pearson's correlation coefficient for the correlation between PMI and the p53 optical density scoring of tongue and pancreas

	Correlation coefficient factor (r)	P-value
Tongue	0.98	< 0.001**
Pancreas	0.99	< 0.001**

**Correlation is significant at the 0.01 level

Table (6): Simple and multivariate linear regression to predict PMI from the P53 optical density scoring of the tongue and pancreas.

	Model	Unstandardized Coefficients		Standardized Coefficients	T	Sig.	Adjusted R^2
		B	Std. Error	Beta			
1	Constant	0.406	0.088		4.608	<0.001*	96.9%
	tongue	5.820	0.217	0.985	26.881	<0.001*	
	PMI = 0.406+ 5.820*P53 optical density scoring of tongue						
2	Constant	0.805	0.055		14.712	<0.001*	98.3%
	pancreas	4.336	0.117	0.992	37.031	<0.001*	
	PMI = 0.805 +4.336*P53 optical density scoring of the pancreas						
3	Constant	0.670	0.077		8.690	.<0.001*	98.6%
	Tongue	1.781	0.774	0.301	2.300	0.032*	
	Pancreas	3.042	0.573	0.696	5.310	<0.001*	
	PMI=0.670 +(1.781*P53 optical density scoring of tongue) + (3.042*P53 optical density scoring of pancreases)						

*Significant p-value < 0.05.

Pancreas histological and immunohistochemical results.

Histological examination of H&E-stained pancreas sections at 0 hours PM revealed the pancreatic acini, where cells had basal basophilic cytoplasm, apical acidophilic granules, and a basal pale vesicular nucleus. Islets of Langerhans were visible and formed by acidophilic cells and basophilic cells (Fig. 3A). At 12 h; the examined pancreatic sections revealed pancreatic acini with karyolysis. The islets were visible with pyknosis (Fig. 3B).

Twenty-four hours after death, a microscopic examination of the pancreatic section from group III showed pancreatic acini with pyknosis and karyolysis. An area of disorganized cells and inflammatory cellular infiltration appeared. The cells of the islets appeared with karyolysis (Fig. 3C). At 48 hours PM, examination of pancreatic sections revealed little acini and only disorganized cells with mostly nuclear ghosts (Fig. 3D).

Immunohistochemically stained sections of the pancreas excised immediately after death presented scarce cytoplasmic reactivity along acinar cells to the p53 antibody (Fig. 4A). At 12 h, sections of the pancreas exposed acinar cells with moderate expression of the p53 antibodies as a cytoplasmic reaction (Fig. 4B). At 24 hours, sections of the pancreas showed high cytoplasmic reactivity of acinar cells to the p53 antibody (Fig. 4C). At 48 hours PM, there was strong cytoplasmic reactivity of the p53 antibody across all pancreatic tissue (Fig. 4D).

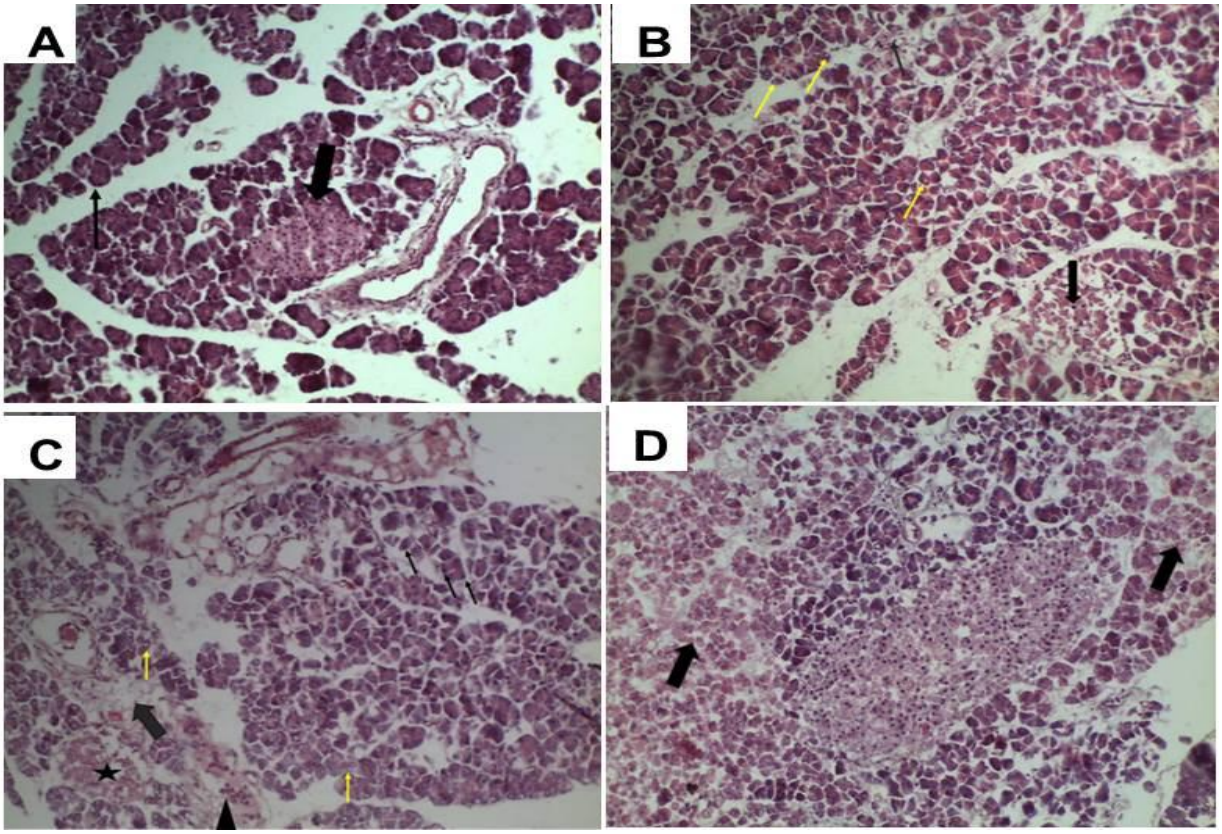

Figure (3): Histological changes of the pancreas at different postmortem intervals.

(A): A photomicrograph of the pancreatic section of an adult male rat from group I, showing pancreatic acini (thin arrow) and islets of Langerhans (thick arrow). (H & E stain x 200).

(B): A photomicrograph of the pancreatic section of an adult male rat from group II showing pancreatic acini with karyolysis (yellow arrow). The islets were visible with pyknosis (a thick arrow). An area of degenerated cells appeared (thin arrow). (H & E stain x 200).

(C): A photomicrograph of a pancreatic section of an adult male rat from group III showing pancreatic acini with pyknosis and karyolysis (yellow arrow). An area of dissociated cells appeared (thick arrow). Inflammatory cellular infiltration appeared (arrowhead). The cells of the islets appeared with karyolysis (a star). (H & E stain x 200).

(D): A photomicrograph of the pancreatic section of an adult male rat from group IV showing little acini and only disorganized cells, mainly with nuclear ghosts (thick arrow). (H & E stain x 200)

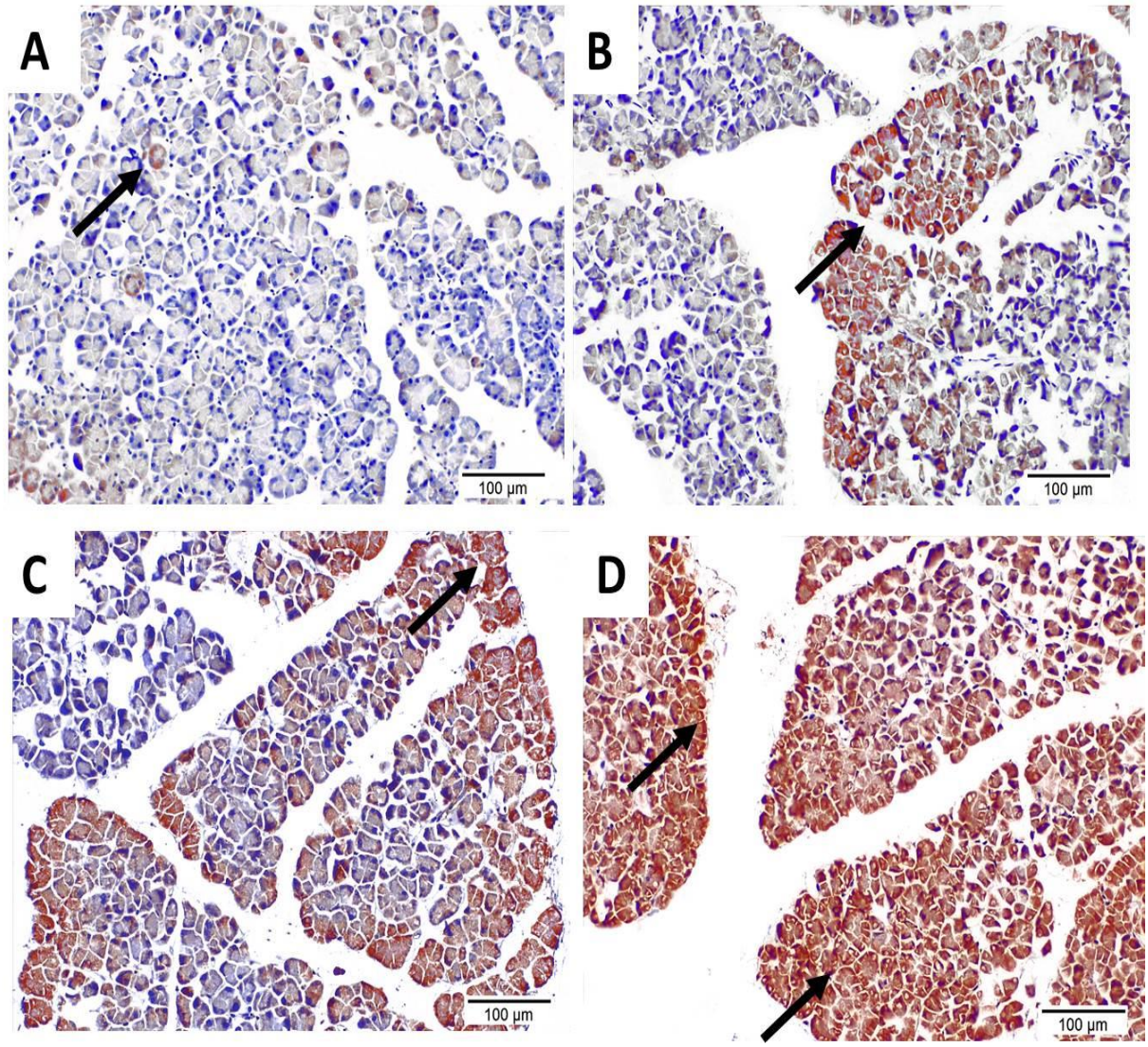

Figure (4): Photomicrographs display the reactivity of the P53 antibody on pancreatic tissues between the assessed groups.

(A): A section of the pancreas in group I presented scarce cytoplasmic reactivity along the acinar cells to the p53 antibody (arrow).

(B): A section of the pancreas in group II exposed acinar cells with moderate expression of the p53 antibody as a cytoplasmic reaction (arrows).

(C): A section of the pancreas in group III showed high cytoplasmic reactivity of acinar cells to the p53 antibody (arrows).

(D): A section of the pancreas in group IV underscored the strong cytoplasmic reactivity of the p53 antibody across all pancreatic tissue (arrows). (P53 antibody, magnification power = x200, and scale bar = 100 m).

With increasing PMI, the optical density score values of p53-positive pancreatic cells statistically significantly increased (Table 4, Graph 2). A significant positive correlation (r 0.99, p-value < 0.001) was observed between the pancreatic p53 optical density score and PMI. (Table 5).

Simple linear regression was utilized to generate the equation PMI = 0.805 + 4.336 * P53 optical density scoring of the pancreas (Adjusted R2 = 98.3%). With a higher Adjusted R2 (98.6%), another equation was derived by multivariate linear regression to predict PMI from both the tongue and pancreatic p53 optical density scores. PMI = 0.670 + (1.781 * P53 tongue optical density scoring) + (3.042 * P53 pancreas optical density scoring) (Table 6).

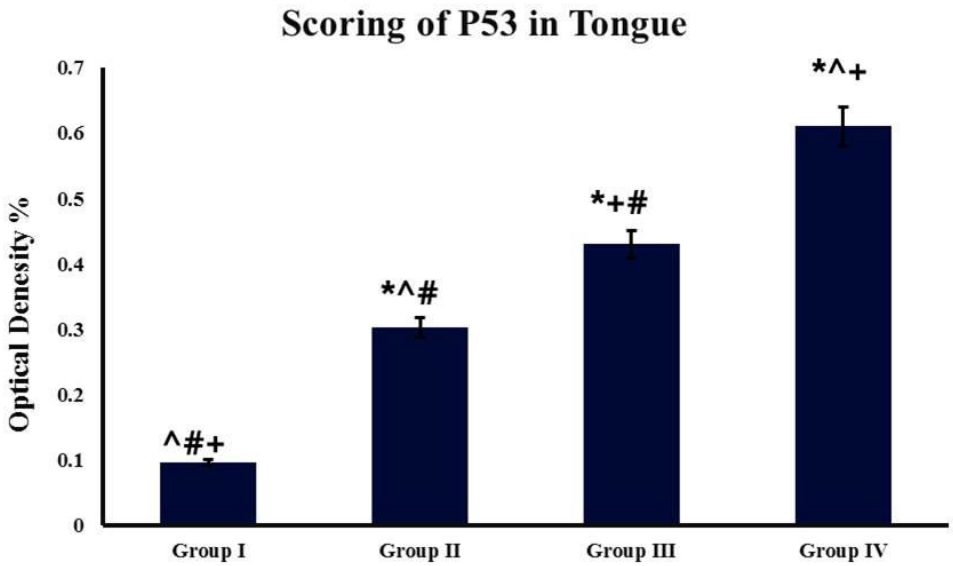

Graph (1): explains the optical density scoring values, which are expressed as mean ± SD. * refers to a significant difference from group I; + refers to a significant difference from group II; ^ refers to a significant difference from group III; and # refers to a significant difference from group IV. A significant difference was presented at $p < 0.001$.

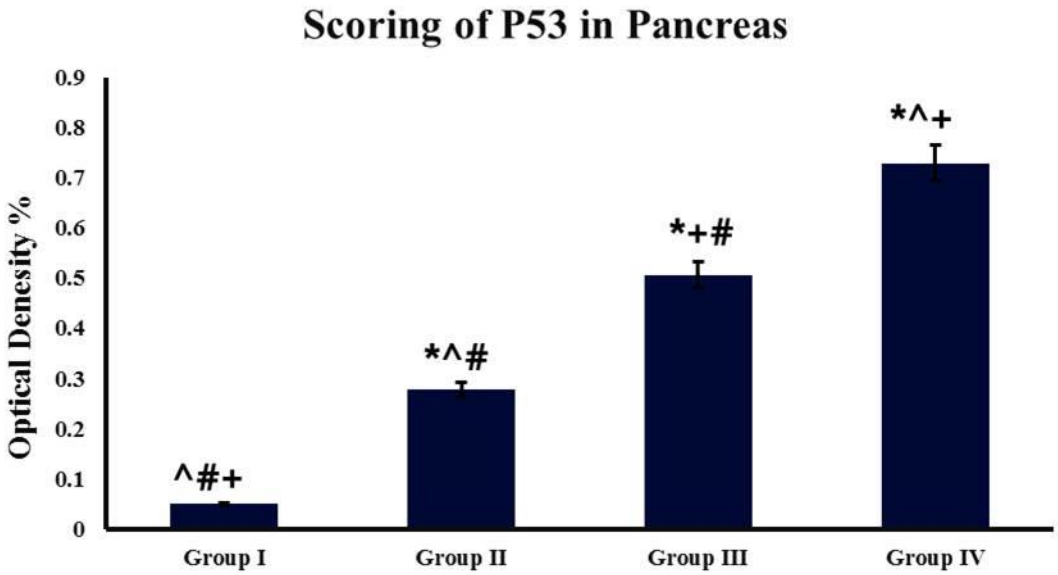

Graph (2): explains the optical density scoring values, which are expressed as mean ± SD. * refers to a significant difference from group I; + refers to a significant difference from group II; ^ refers to a significant difference from group III; and # refers to a significant difference from group IV. A significant difference was presented at $p < 0.001$.

DISCUSSION

For determining the postmortem interval, the current study employed three distinct approaches: blood biochemical alterations (uric acid, lactate, amylase, lipase, and insulin levels) and histological and immunohistochemical changes affecting the tongue and pancreas.

Several biochemical indicators have been discovered to be extremely stable following death, whereas others alter to varied degrees**.** Oxygen deprivation, the ongoing progress of chemical interactions in the early stages of the postmortem period, and the dispersion of easy diffusible compounds between red cells and plasma in addition to within the interstitium, tissue, and blood are three factors that contribute to the biochemical changes that occur **(Buras, 2006)**.

Immediately after death or shortly after, postmortem chemical modifications occur in the body and proceed until the corpse

disintegrates. Every modification happens at a distinct speed. Determining the chemical alterations might aid forensic pathologists in more precisely determining the period since death **(Mahmoud et al., 2018, Yahia and Abdel-Hakiem, 2014).**

In the current study, the mean value of serum uric acid in groups II, III, and IV showed a significant statistical increase compared to group I. Moreover, a significant moderate positive correlation existed between serum uric acid levels and the postmortem interval.

Uric acid is generated as a byproduct of the purine metabolism. The rise of uric acid after death may be explained by the release of purine during the disintegration of white blood cells (WBCs), which xanthine oxidase then converts into uric acid **(Donaldson and Lamont, 2013).**

The current study's findings corroborated those of **Donaldson and Lamont (2013),** who reported increased serum uric acid concentration. It multiplied five times 96 hours after death. On the other hand, **Srettabunjong et al. (2020)** observed that serum uric acid levels in blood were not significantly linked to PMI. The shorter research span may have contributed to the divergent outcomes. They only tracked uric acid levels for 15 hours following death, which may not have been long enough to notice a significant difference between blood uric acid levels during the antemortem and postmortem periods. Also, the blood samples were obtained from the deceased from the jugular vein, which differs from the present study.

Lactate is the byproduct of glucose's anaerobic metabolism (**Rabinowitz and Enerbäck, 2020).** Compared to group I, the mean value of serum lactate in groups II, III, and IV showed a significant statistical increase. In addition, blood lactate levels and the time since death were strongly positively correlated.

These findings may be explained by the transition to anaerobic metabolism brought on by the decrease in oxygen concentration following death, leading to lactic acid accumulation **(Kushimoto et al., 2016).**

These results align with **Szeremeta et al. (2023)**, who found that lactic acid was among the PMI's most potential metabolic markers. Also, In vitro, blood samples of rats showed rising lactate concentrations over time, as **Donaldson and Lamont (2013)** reported. However, the level did not rise linearly; the lactate levels first markedly dropped at 24 hours before going up until 96 hours.

The pancreas releases the digestion enzyme amylase. Its primary function is to convert carbohydrates into simple sugars **(Sanchez and Demain, 2017).** The mean value of serum amylase in the various groups did not significantly differ in the current study. Moreover, there was no correlation between serum amylase and the time since death.

Compared to the results of the present investigation, **Brown and Prahlow (2018)** reported higher serum amylase after death, which may be a sign that acute pancreatitis was the cause of death. The present study did not consider acute pancreatitis as a cause of mortality. However, throughout the 250 hours after sample collection, **Campos et al. (2014)** found that the serum amylase content was considerably reduced. The fact that they utilized human blood samples at various temperatures might cause disparate outcomes.

A pancreatic enzyme called lipase is required for the digestion of food and absorption **(Zhu et al., 2021).** In the current investigation, groups III and IV had significantly higher mean serum lipase levels than group I. Moreover, a moderate, positive correlation existed between its levels and the time since death.

The findings may be explained by lipase being kept inside pancreatic cells, which release their intracellular supply of lipase into the blood when the pancreas is harmed by putrefaction **(Buras, 2006).**

Brown and Prahlow (2018) observed high postmortem serum lipase up to 68 hours after death, which was explained by acute pancreatitis as a cause of death. Nevertheless, **Campos et al. (2014)** discovered that lipase concentration stays consistent throughout the 250 hours following collection. The varying results might be due to different methodologies, as aforementioned.

Insulin is a polypeptide hormone. The pancreatic islets of Langerhans are where insulin is mostly produced. In the bloodstream, it controls blood glucose levels **(Rahman et al., 2021).** The mean value of serum insulin in each group in the current study did not differ statistically from one another. Moreover, the correlation between its levels and the postmortem period was non-significant.

These findings might be attributed to insulin stored in β-cells as tightly packed crystalline, insoluble hexameric insulin granules. At room temperature, it is stable and starts to decay four to five days after death **(Labay et al., 2016).**

Kumar and Verma (2016) observed the opposite outcomes, concluding that there was a significant correlation between insulin levels and PMI. They reported that insulin levels dropped during a postmortem period of up to 27 hours. They explained their results by the thiol groups of hemoglobin, which cleave the disulfide bonds of insulin and promptly produce new intramolecular disulfide bridges in hemolytic blood.

Local oxygen consumption increases quickly without blood flow, which causes a switch to anaerobic metabolism. The energy-dependent cellular systems cease to operate when all locally available nutrients are gradually catabolized by anaerobic mechanisms, resulting in permanent alterations to the organic structures **(Hostiuc et al., 2017).** Postmortem interval estimation can benefit from time-related histological examination of diverse organs and tissues **(Agarwal et al., 2016).**

In the present study, histological examination of tongue tissue at different postmortem intervals showed epithelial shredding and splitting in the tongue tissue and cytoplasmic eosinophilia. With increasing postmortem intervals, cytoplasmic vacuolation, karyolysis, pyknosis, and karyorrhexis were found throughout the epithelium. Also, there was extensive muscle degeneration.

These findings might be explained by hypoxia when the vital processes ceased, causing substantial cell damage and cell death. The cell died due to mitochondrial malfunction, lysosomal membrane breakdown, and enzymatic activity **(Vavpotic et al., 2009).** The current study findings were consistent with **Rajkumari et al. (2020)**, who noted gradual autolytic modifications of the tongue in the form of architectural, nuclear, and cytoplasmic abnormalities.

In the present study, histological examination of the pancreas at different postmortem intervals showed that pancreatic acini appeared at first slightly vacuolated, then, with increasing postmortem intervals, they appeared with dark nuclei and nuclear ghosts (karyolysis). Also, islets of Langerhans were visible at first and formed by acidophilic and basophilic cells, and with increasing postmortem intervals, they appeared with dark nuclei and nuclear ghosts.

The present study's histological changes were caused by postmortem anoxic outcomes such as ischemia, glycolysis, and proteolysis. Furthermore, releasing lysosomal autolytic enzymes results in the breakdown of cellular components and the destruction of tissue architecture **(Miller and Zachary, 2017).**

The current study concurred with those of **Khalifa et al. (2022),** who discovered that pancreatic slices of rats stained with H&E 72 hours after death revealed significant regions of damaged cells, and no acini could be seen.

A wide range of cellular stressors causes p53, a sequence-specific transcription factor, to rise rapidly, stimulating the activation of numerous genes that cause cell death. **(Nair et al., 2006)**

In the present study, scarce cytoplasmic reactivity to p53 antibody in skeletal muscle cells of the tongue and pancreatic tissue was reported at 0-hour pm, with increasing immunohistochemical reactivity to the anti-p53 antibody with increasing PMI. There was a strong positive correlation between p53 optical density scoring of the tongue, pancreas, and PMI.

The increasing immunohistochemical reactivity could be clarified by interrupting breathing and circulation during death, causing tissue ischemia and anoxia. As a result, p53 is activated during the first few hours of death, which causes Apoptosis. **(Hanna et al., 2021**).

Khalifa et al. (2022) reported a similar finding. They observed that adult male albino rats' pancreas had substantial positive relationships between P53 and PMI. Similar results were obtained by **Mohamed et al. (2017),** who investigated the postmortem immunohistochemistry expression of p53 at a variety of intervals (0, 6, and 12 PM) in the rabbits' brains. They discovered that when PMI rose, so did the expression of p53.

Hanna et al. (2021) discovered, in contrast to the results of the current investigation, that albino rat skeletal muscle p53 showed a very strong negative connection with PMI as the p53 expression level steadily declined regardless of the PMI. Additionally, research by **Lee et al. (2016)** found that p53 expression levels in rat kidneys and psoas muscles remained stable for at least 96 hours

after death. Different methods may account for the various outcomes. Carbon dioxide gas was used to suffocate the rats and cause their deaths.

In this work, equations for calculating PMI were derived from linear regression analyses of lactate and the pancreatic and tongue P53 optical density scores.

Analyses using simple linear regression were significant for each. However, the outcome of using multiple linear regression analysis of the pancreatic and tongue P53 optical density scores to predict PMI was superior to that of the simple one, with a high adjusted R^2. There was no literature available to compare these findings against.

CONCLUSIONS

Lactate, lipase, and serum uric acid correlate positively with PMI. The postmortem interval may be calculated using the blood lactate level by the regression formula: PMI = 0.052 + 0.111 (serum lactate). The histological analysis of the tongue and pancreas revealed an ongoing deterioration throughout the postmortem period. The present study concluded that p53 expression in the tongue and pancreas showed a significantly strong positive correlation with PMI. So, utilizing formulas of simple and multiple linear regression analyses, we may predict PMI using the p53 optical density score with high reliability.

RECOMMENDATIONS:

- It is recommended to apply the useful results of the current study in determining PMI.
- It is advised to conduct more research to check the accuracy of the postmortem interval determination by histological and immunohistochemical analysis of various bodily organs and the evaluation of additional biochemical indicators.
- Also, it is advised to research the impact of several elements not addressed in this study on the postmortem autolytic process (such as the method and cause of death, the temperature, and other environmental factors, as well as the air humidity).
- Even though this animal study produced impressive results, more research on humans is required.

List of abbreviations

PM: postmortem; PMI: Postmortem interval; EDTA: ethylene diamine tetra acetic acid; ELISA: The enzyme-linked immunosorbent assay; H&E: Hematoxylin & Eosin; IHC: Immunohistochemistry; ABC: avidin-biotin-peroxidase complex; DAB: diaminobenzidine; ANOVA: analysis of variance; SPSS: Statistical Package for Scientific Studies;

Conflict of interest: The authors declare that they have no competing interests.

Funding: None.

Acknowledgment: Not applicable.

REFERENCES

Abdelaleem, S.A.; Younis, R.H. and Ahmed, R.F.(2016): Postmortem interval estimation using myoglobin concentration in different glandular tissues. International Journal of Forensic Science and Pathology, 4:259-265

Agarwal, S.; Chaudhary, M.; Gawande, M. and Gupta, P. (2016): Documentation of postmortem changes in salivary gland architecture and staining characteristics. Journal of Forensic Dental Sciences, 8(2): 113-118.

Brooks, J.W. and Sutton, L. (2018): Postmortem changes and estimating the postmortem interval. In: Veterinary forensic pathology, 1st ed, Vol 1. Springer Cham, Switzerland, pp 43–63.

Brown, T.T. and Prahlow, J.A. (2018): Postmortem serum amylase and lipase analysis in the diagnosis of acute pancreatitis. Academic Forensic Pathology, 8(2): 311–323.

Buras, K.L. (2006): Are enzymes accurate indicators of postmortem interval? A biochemical analysis. LSU Master's Theses 177.

Campos, C.M.O.; Silvestre, D.R.J. and Oliveir, D.R.J. (2014): Estimating the postmortem interval by clinical chemistry. Advanced Institute of Health Science 35-37.

Cordeiro, C.; Ordonez-Mayan, L.; Lendoiro, E.; Febrero-Bande, M.; Vieira, D.N. and Barus, JM (2019): A reliable method for estimating the postmortem interval from the biochemistry of the vitreous humor, temperature, and body weight. Forensic Sci. Int., 295: 157–168.

Donaldson, A.E. and Lamont, I.L. (2013): Biochemistry changes that occur after death: Potential markers for determining postmortem interval. PLoS ONE 8(11): e82011.

Elvas, F.; Vanden Berghe, T.; Adriaenssens, Y.; Vandenabeele, P.; Augustyns, K. Staelens, S. et al. (2019): Caspase-3 probes for PET imaging of apoptotic tumor response to anticancer therapy. Organic & biomolecular chemistry; 17(19):4801-4824.

Hanna, M.M.; Abd El Wahab, S.A.; Adel, R. and Ahmed, A.M.(2021): Immunohistochemical markers study from different organs of rats after death for estimation of postmortem interval: An experimental study. MJMR, 32(2): 80-90.

Hostiuc, S.; Rusu, MC; Mănoiu, V.S.; Vrapciu, A.D.; Negoi, I. and Popescu, M.V. (2017): Usefulness of ultrastructure studies for the estimation of the postmortem interval. Romanian Journal of Morphology and Embryology, 58(2): 377–384.

Khalifa, F.N.; Hosny, SA and Moawad, A.M. (2022): Histobiochemical changes in early postmortem interval in liver, pancreas, skin, and kidney of adult male albino rats. Rechtsmedizin, 32(1): 4-11.

Kumar, S. and Verma, A.K. (2016): Estimation of postmortem interval using the data of insulin level in the cadaver′s blood. Data in Brief, 7: 354–356.

Kushimoto, S.; Akaishi, S.; Sato, T.; Nomura, R.; Fujita, M.; Kudo, D. et al. (2016): Lactate, a useful marker for disease mortality and severity but an unreliable marker of tissue hypoxia and hypoperfusion in critically ill patients. Acute Med Surg 3(4): 293–297

Labay, L.M.; Bitting, C.P.; Legg, K.M. and Logan, B.K. (2016): The determination of insulin overdose in postmortem investigations. Acad. Forensic Pathol., 6(2):174-183.

Lee, D. G.; Yang, K. E.; Hwang, J. W.; Kang, H. S.; Lee, S. Y.; Choi, S. et al. (2016): Degradation of kidney and psoas muscle proteins as indicators of postmortem interval in a rat model, with use of lateral flow technology. PloS one; 11(8): e0160557.

Mahmoud, N. A.; Hassan, A. A; Abdel Rahim, A. H.; Mahmoud S. M. and Nada, O.H. (2018): Molecular versus histopathological examination of the prostate gland in the estimation of postmortem interval (An experimental study) Egypt J. Forensic Sci. Appli. Toxicol., 18 (1):35-54.

Miller, M.A. and Zachary, J.F. (2017): Mechanisms and Morphology of Cellular Injury, Adaptation, and Death. Pathologic Basis of Veterinary Disease, 2–43.e19.

Mohamed, A.A.; Elbohi, K.M.; Sharkawy, N.I. and Hassan, M.A. (2017): Biochemical and apoptotic biomarkers as indicators of time elapsed since death in experimentally induced traumatic brain injury. SM Journal of Forensic Research and Criminology,1(2):1010.

Mohamed, S.A; Radwan, R.A. El Nashar, A.T.; Salama, E.; Adel, S.M. (2020): Studying histopathological changes in suprarenal gland versus vitreous humor potassium level in estimation of postmortem intervals: experimental study in rabbits Egypt J. Forensic Sci. Appli. Toxicol., 20(2): 61-72.

Nair, V. D.; McNaught, K. S.; González-Maeso, J.; Sealfon, S. C. and Olanow, C. W. (2006): p53 mediates non-transcriptional cell death in dopaminergic cells in response to proteasome inhibition. The Journal of biological chemistry, 281(51): 39550–39560.

Onyejike, D.N.; Fischer, V.A.; Esomonu, U.G.; Nwamaradi, A.T. and Onyejike, I.M. (2022): Factors that influence decomposition timeline estimation in Anambra state, Nigeria. Egypt. J. Forensic Sci., 12, 29.

Rabinowitz, J.D. and Enerbäck, S. (2020): Lactate: the ugly duckling of energy metabolism. Nature Metabolism, 2(7):566-571.

Rahman, M.S.; Hossain, K.S.; Das, S.; Kundu, S.; Adegoke, E.O.; Rahman, M.A. et al. (2021): Role of insulin in health and disease: an update. International Journal of Molecular Sciences, 22(12):1-19.

Rajkumari, S.; Mensudar, R.; Naveen, N.; Thayumanavan, B. and Thammaiah, S. (2020): Estimation of postmortem death interval from autopsied tongue tissue: A cross-sectional study. Journal of Oral and Maxillofacial Pathology, 24(3): 568–571.

Sanchez, S. and Demain, A. (2017): Useful microbial enzymes-an introduction. In: Brahmachari G, Demain A, Adrio J (eds) Biotechnology of microbial enzymes, 1st ed, Ch 1. Academic Press, San Diego, CA, pp 1-11.

Srettabunjong, S.; Thongphap, W. and Chittamma, A. (2020): Urea, uric acid, and creatinine in postmortem blood, vitreous humor, and synovial fluid: a comparative and correlation study. Journal of Forensic Sciences, 65(1): 128–133

Szeremeta, M.; Samczuk, P.; Pietrowska, K.; Kowalczyk, T.; Przeslaw, K.; Sieminska, J. et al. (2023): In vitro animal model for estimating the time since death with attention to early postmortem stage. Metabolites, 13, 26. https://doi.org/10.3390/ metabo13010026

Tang, T. and Zhang, D. L. (2017): Detection of p53 and Bcl-2 expression in cutaneous hemangioma through the quantum dot technique. Oncology letters, 13(5): 2937–2944.

Vavpotic, M.; Turk, T.; Martincic, D.S. and Balazic, J. (2009): Characteristics of the number of odontoblasts in human dental pulp postmortem. Forensic Science International, 193(1-3): 122–126.

Welson, NN; Shereen, S.; Gaber, S.S.; Batiha, G.E. and Ahmed, S.M. (2021): Evaluation of time passed since death by examination of oxidative stress markers, histopathological, and molecular changes of major organs in male albino rats. International Journal of Legal Medicine, 135(4):269-280.

Yahia, D. and Abdel-Hakiem, M. (2014): Biochemical analysis of synovial fluid, cerebrospinal fluid, and vitreous humor at early postmortem intervals in donkeys. Journal of Advanced Veterinary Research, 4(1): 6-11.

Zhu, G.; Fang, Q.; Zhu, F.; Huang, D. and Yang, C. (2021): Structure and function of pancreatic lipase-related protein 2 and its relationship with pathological states. Frontiers in Genetics, 12: 35-38.

الملخص العربى

تقييم التغيرات الكيميائية والنسيجية وتعبير الأنسجة عن P53 كمؤشر لتحديد الفترة الزمنية المبكرة بعد الوفاة في ذكور الجرذان البيضاء البالغة

سارة السيد قاسم[1]. سهير علي محمد[1]. سميرة محمود محمد[2]. مارتينا اوسام خلف[1]. احمد محمد سعيد[1]

[1] قسم الطب الشرعي والسموم الاكلينيكية، [2] قسم الهستولوجيا وبيولوجيا الخلية، كلية الطب، جامعة سوهاج

مقدمة: تقدير الفترة منذ الوفاة هو الأولوية الأولى للطب الشرعي. ويساعد التحقيقات القضائية الأخرى في فهم الموقف ومحاسبة المجرمين المحتملين. **هدف الدراسة:** يهدف البحث الحالي الي تقييم دور الوسائل المختلفة في تقدير فترة ما بعد الوفاة من خلال دراسة التغيرات البيوكيميائية في الدم (مستويات حمض اليوريك ، اللاكتات ، الأميليز ، الليبيز، والأنسولين) ، والتغيرات النسيجية ، والتعبير الكيميائي النسيجي المناعي للجسم المضاد p53 في اللسان والبنكرياس. **منهج الدراسة:** استُخدم أربعون فأراً من ذكور الجرذان البيضاء البالغة في الدراسة الحالية. وفقًا لفترات ما بعد الوفاة المتنوعة ، تم تقسيم الحيوانات إلى أربع مجموعات بشكل عشوائي: 0 ساعة ، و 12 ساعة ، و 24 ساعة ، و 48 ساعة بعد الموت. **النتائج:** أظهرت مستويات حمض اليوريك في الدم واللاكتات والليبيز ارتباطًا إيجابيًا بفترة بعد الوفاة. يمكن توقع فترة ما بعد الوفاة باستخدام صيغة الانحدار التي تستخدم مستوى اللاكتات في الدم. يمكن ملاحظة التغيرات النسيجية في انسجة البنكرياس واللسان، وكذلك زاد التعبير الكيميائي النسيجي المناعي للجسم المضاد p53 بشكل تدريجي خلال فترة ما بعد الوفاة. **الاستنتاج:** القدرة على تحديد المدة التي مرت بعد الوفاة أمر ضروري في الطب الشرعي. مستوى اللاكتات في الدم هو أدق المعايير البيوكيميائية التي درست في هذا البحث. بالإضافة إلى ذلك، يمكن استخدام صيغ الانحدار باستخدام درجات الكثافة الضوئية للسان والبنكرياس للتنبؤ بفترة ما بعد الوفاة، بمزيد من الدقة عند استخدامها معًا.